Cloud-Aerosol Lidar and Infrared Pathfinder Satellite Observations (CALIPSO)

Algorithm Theoretical Basis Document

Level 1, Wide Field Camera (WFC)

The CALIPSO WFC Science Working Group

Version 2.0
October 15, 2004

Table of Contents

1. INTRODUCTION

1.1 Purpose

The intent of this document is to describe the Level 1 data processing algorithms for the Cloud-Aerosol Lidar and Infrared Pathfinder Satellite Observations (CALIPSO) satellite mission's Wide Field Camera (WFC) instrument. These algorithms will convert the WFC outputs from raw digital counts and engineering units into geolocated, radiometric parameters that make up the Level 1 data product. The digital counts and engineering units are referred to as the Level 0 data product. These algorithms are part of the CALIPSO WFC Level 1 subsystem that operates at the Langley Atmospheric Sciences Data Center.

1.2 Scope

This document serves to describe the major processing tasks implemented in the Level 1 WFC processing software. The description of the processing tasks includes lists of the inputs and outputs to each algorithm, mathematical descriptions of the algorithms, top-level flow diagrams, and discussions of practical implementation issues.

1.3 CALIPSO Reference Documents

This section should list all relevant CALIPSO documents including IIR ATBD, Data Products Catalog, etc.

1.4 Revision History

This is Version 2.0 of this document. Revisions must be approved by the CALIPSO Principal Investigator and Wide Field Camera Instrument Scientist.

2. CALIPSO MISSION OVERVIEW

2.1. Introduction

Current uncertainties in the roles played by clouds and aerosols in the Earth radiation budget limit our understanding of the climate system and the potential for global climate change. Cloud-Aerosol Lidar Infrared Pathfinder Satellite Observations (CALIPSO) is a recently approved satellite mission within NASA's Earth System Science Pathfinder (ESSP) program (formerly the PICASSO-CENA mission) which will address these uncertainties with a unique suite of active and passive instruments.

The Lidar In-space Technology Experiment (LITE) demonstrated the potential benefits of space lidar for studies of clouds and aerosols (Winker et al., 1996). The CALIPSO mission builds on this experience with a payload consisting of a two-wavelength polarization-sensitive lidar, and passive imagers operating in the visible and infrared spectral regions. Data from these instruments will be used to measure the vertical distributions of aerosols and clouds in the atmosphere, as well as optical and physical properties of aerosols and clouds which influence the Earth radiation budget.

CALIPSO will be flown in a polar orbit as part of the Aqua Constellation, which also includes the Aqua and Aura (formerly EOS PM and EOS Chem) satellites, and the CloudSat and PARASOL satellites. Aqua carries a suite of instruments, including the MODIS, CERES and AIRS instruments, designed to study the Earth hydrologic cycle. CloudSat carries a 94 GHz cloud radar to provide cloud profiles and cloud physical properties. PARASOL is a satellite being developed by the French space agency CNES which will provide multi-spectral, multi-angle and polarization measurements of clouds, aerosols, and the Earth's surface.

The five satellites of the constellation will, together, provide an unprecedented, comprehensive suite of coincident measurements of atmospheric state, aerosol and cloud optical properties, and radiative fluxes. This combined dataset will allow fundamental advances in our understanding of the links between aerosols, clouds, and radiation necessary to more accurately assess future climate change.

CALIPSO is planned for launch in 2004, followed by a three year on-orbit mission. CALIPSO is being developed within the framework of a collaboration between NASA and CNES.

2.2 Science Objectives

CALIPSO will address critical uncertainties in the direct radiative forcing of aerosols and clouds as well as aerosol influences on cloud radiative properties and cloud-climate radiation feedbacks.

Atmospheric aerosols *directly* affect the Earth's energy balance by absorbing and scattering shortwave (SW) solar radiation, and by absorbing and emitting longwave (LW) infrared radiation. Aerosols *indirectly* affect this balance by modifying the reflectance and lifetime of clouds through their role as cloud condensation nuclei, but this indirect forcing is poorly quantified. Unlike greenhouse gases, tropospheric aerosols are highly variable in space and time due to variable sources and short atmospheric residence times. Thus their radiative effects are also highly variable. The uncertainties in these effects may be more than half the entire greenhouse gas effect, but of opposite sign.

Current observationally-based estimates of global aerosol forcing are severely handicapped by the current limited capabilities to observe aerosol from space. However, models must be used to estimate the impacts of aerosols on the climate in the past and to predict future trends. Model estimates of aerosol forcing, even forcing of the current climate, are highly uncertain, largely because current capabilities to observe the global distribution and properties of aerosols are insufficient to constrain key assumptions in these models. CALIPSO will provide critical observations of the vertical distribution of aerosols, an ability to perform height-resolved discrimination of aerosol into several types, and an improved capability to observe aerosol over bright and heterogeneous surfaces.

The sensitivity of the climate to external forcings is largely controlled by interactions between clouds and radiation. Advances in model capabilities to predict climate change requires improved representations of cloud processes in models and decreased uncertainties in cloud-radiation interactions. The fundamental problem is in modeling the cloud feedback loop shown in Figure 2.1. The largest uncertainties involve the use of models to (a) predict cloud properties based on atmospheric state, and (b) use of these cloud properties to calculate radiative energy fluxes. In particular, the largest source of uncertainty in estimating longwave radiative fluxes at the surface and within the atmosphere are connected with current difficulties in determining the vertical distribution and overlap of multilayer clouds.

Because of the short time scales and nonlinear relationships typical of cloud processes, nearly simultaneous observations of all three parts of the cloud feedback loop shown in Figure 2.1 are necessary to test the ability of cloud models to reproduce the physics of cloud-radiation feedbacks. Simultaneous, coincident data from CALIPSO, Aqua, CloudSat, and PARASOL will allow the most complete closure of this feedback loop possible in the near future.

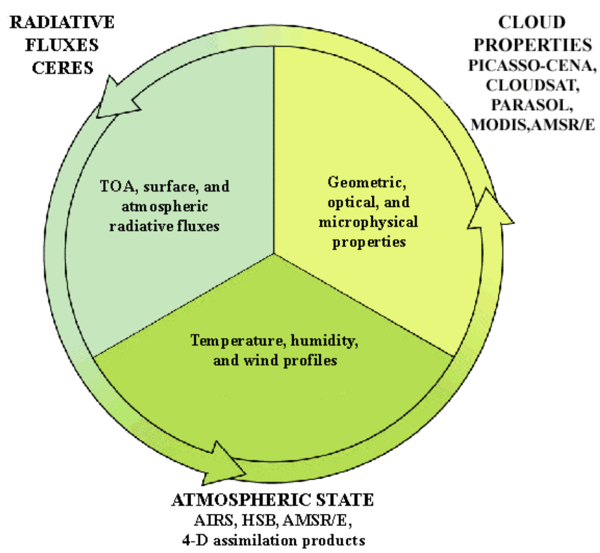

Figure 2.1. Connections between atmospheric state, cloud properties, and radiative fluxes and the instruments required to observe the relevant parameters.

2.3. Instruments

The CALIPSO lidar is a two-wavelength, polarization-sensitive instrument providing high resolution vertical profiles of aerosol and cloud properties. The change in backscatter with wavelength allows the identification of aerosol populations dominated by accumulation mode or coarse mode particles. The ratio of orthogonally polarized components of the 532 nm backscatter allows the identification of cloud ice/water phase and the discrimination of spherical and non-spherical aerosol particles.

The CALIPSO payload also contains two passive instruments: the Imaging Infrared Radiometer (IIR), being developed by CNES; and the Wide Field Camera (WFC); which are both nadir-viewing and co-aligned with the lidar.

- The IIR provides calibrated radiances at 8.7 µm, 10.6 µm, and 12 µm over a 64 km swath. These wavelengths are chosen to optimize joint lidar/IIR retrievals of cirrus emissivity and particle size. Use of a microbolometer detector array in a non-scanning, staring configuration allows a simple and compact design.
- The WFC has a single channel covering the 620 nm to 670 nm spectral region providing images of a 61 km swath with a spatial resolution of 125 meters. Data from the WFC are used in IIR retrievals. The WFC also provides meteorological context for the lidar measurements and allows highly accurate spatial registration between CALIPSO and instruments on other satellites of the Aqua constellation.

Instrument characteristics are summarized in Table 2.2.

Characteristic	Value
Lidar:	
wavelengths	532 nm, polarization sensitive 1064 nm (intensity)
telescope dia.	1 meter
footprint/FOV	100 m/130 µrad
spatial resolution	333 m horiz, 30 m vert
WFC:	
spectral range	620-670 nm
IFOV/swath	125 m/ 61 km
IIR:	
wavelengths	8.7 µm, 10.6 µm, 12.0 µm
spectral resolution	0.8 µm
IFOV/swath	1 km/64 km

Table 2.2. Instrument characteristics.

2.4 Measurements

The data products to be available from CALIPSO and the instruments from which they are obtained are listed in Table 2.3. Lidar cloud data will be used in IIR retrievals to provide an independent estimate of cloud temperature, to identify single- and multi-layer cloud, and to provide improved identification of cloud-free scenes. Processing and archival will be performed at the NASA Langley Research Center DAAC.

Measurement	Lidar	WFC	IIR
Aerosol profiles	•		
Aerosol optical depth	•		
Cloud height and thickness	•		
Cloud optical depth	•		
Cloud ice/water phase	•		
Cirrus emissivity	•	•	•
Cirrus particle size	•	•	•

Table 2.3. CALIPSO aerosol and cloud measurements**.**

2.5 Observing Strategy

The orbit of CALIPSO was chosen to provide space-time coincidence with Aqua observations. Aqua is in a sun-synchronous 705-km circular orbit with an ascending node equatorial crossing time of 13:30 local time. CALIPSO will fly at the same altitude as Aqua, and its orbit will be maintained so that a point on the ground will be observed by the two platforms within a few minutes of each other.

Many synergies can be realized by the combination of data sets to be acquired by the Aqua constellation. Simultaneous observation of aerosol properties by CALIPSO and of radiative fluxes and atmospheric state from Aqua will provide direct measurements of aerosol forcing and the key parameters that control it. Cloud observations from the lidar and the CloudSat radar will be complementary, together encompassing the variety of clouds found in the atmosphere. Improved estimates of surface LW fluxes and atmospheric heating rates will be obtained by combining CERES TOA flux measurements with coincident observations of multilayered clouds from CALIPSO and CloudSat. PARASOL will add multi-angle and polarization measurements of reflected sunlight providing additional capabilities to sense cloud and aerosol properties.

3. WIDE FIELD CAMERA OVERVIEW

3.1 Role of Wide Field Camera in CALIPSO

The CALIPSO WFC is a narrow-band push-broom imager that provides continuous high spatial resolution imagery during the daylight segments of the orbit over a swath centered on the lidar footprint. The WFC swath is illustrated conceptually in Figure 3.1. The spectral band of the WFC is designed to match the Aqua MODIS instrument's channel 1 having a central wavelength of 645 nm and a bandwidth of 50 nm. The primary WFC Level 1 products are radiance and reflectance registered to an Earth-based grid centered on the lidar ground track.

One of the primary uses of the WFC is to accurately co-register CALIPSO images with those from Aqua to facilitate joint CALIPSO/Aqua retrievals. Another important role of the WFC is to provide supplemental data to the IIR retrievals of cloud microphysical properties. For instance, the visible wavelength WFC radiometric data will be utilized to identify the presence of low cloud and assess homogeneity over the IIR footprint. Additional applications of the WFC data will be to provide overall meteorological context to CALIPSO imagery and to verify the pointing accuracy of the CALIPSO platform.

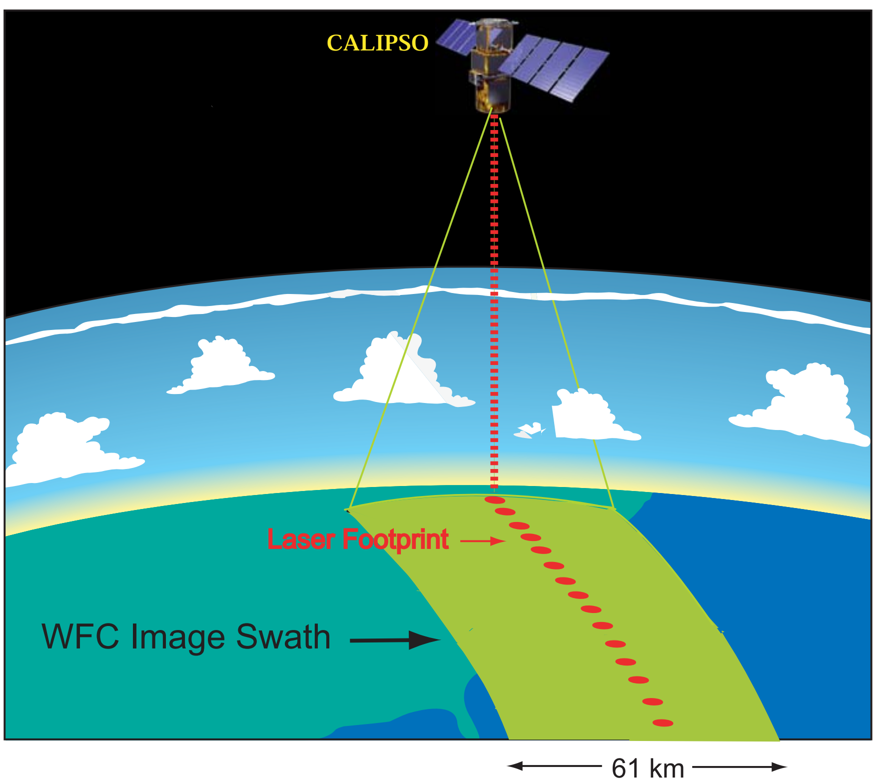

Figure 3.1. WFC image swath.

3.2 WFC Instrument Description

The WFC is a commercial-off-the-shelf instrument based on the Ball Aerospace & Technologies Corporation CT-633 star tracker design. Although the WFC is designed with a 512 x 512 CCD array, it essentially operates as a push broom line camera by reading out only one row of pixels per image frame (see Figure 3.2). Nominally, 488 of the 512 pixels in the target row are utilized. To minimize smearing during readout operations, most of the CCD is masked off except approximately 30 rows near the center. This masking is accomplished by applying an opaque coating to the inside of the CCD window. If necessary, the active row can be reprogrammed on-orbit.

The IFOV of each pixel in the camera is approximately 125 m x 125 m when projected onto the Earth's surface from a nominal 705 km orbit. The image plane is oriented such that the active row of pixels is aligned in the cross track direction providing a full swath FOV of approximately 61 km in the cross track direction centered on the lidar boresight. Pixels outside the central 5-km cross-track swath are averaged to produce low-resolution (1 km) image samples. The resultant single frame data consists of two low-resolution swaths (each 28-km wide) on either side of a high-resolution swath (5-km wide) centered on the lidar ground track. Figure 3.3 shows schematically how the WFC images are built by accumulating these single frames along the orbit track.

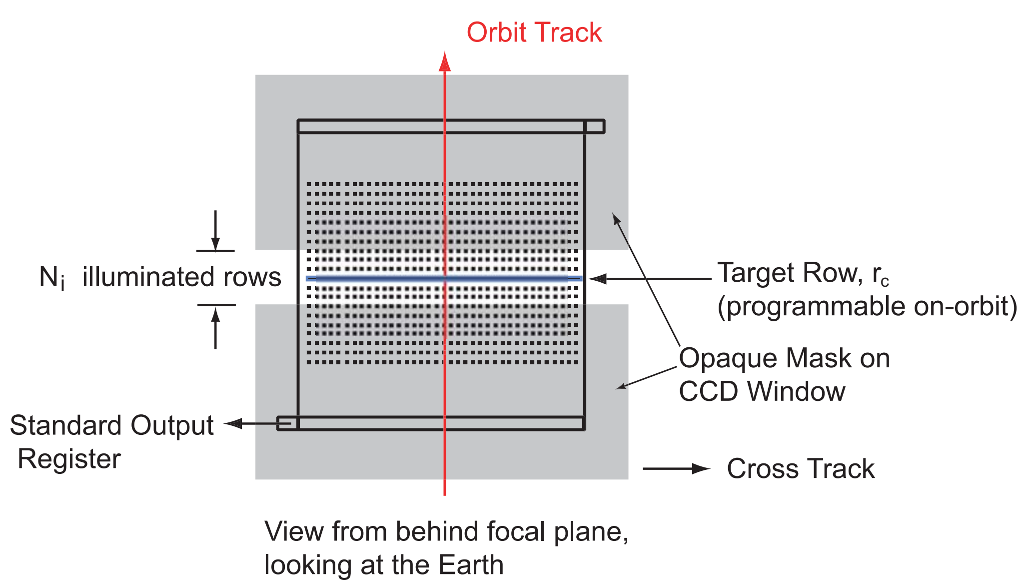

Figure 3.2. WFC operates as a pushbroom scanner.

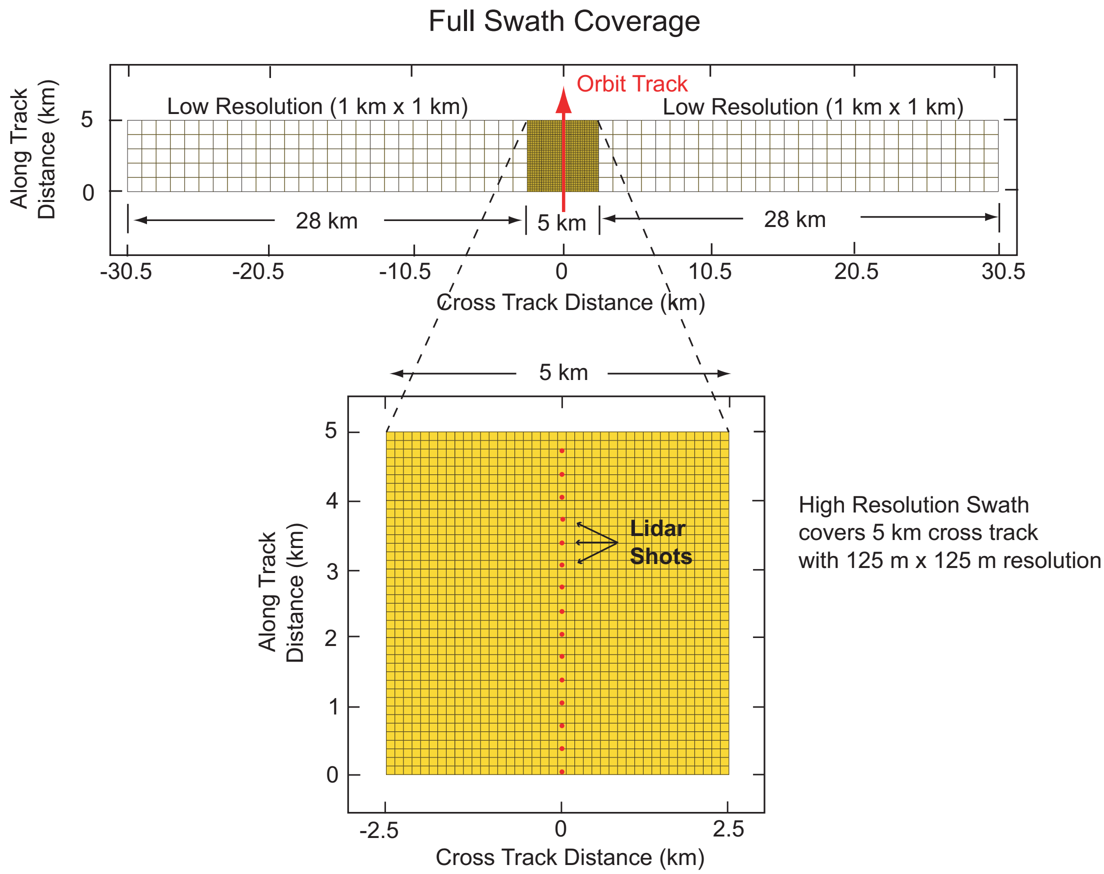

Figure 3.3 Single WFC frames are accumulated along-track to build images.

The WFC is designed to have a large dynamic range that will allow it to observe bright clouds without saturation and still be able to detect small variations in surface albedo. Although there is not a requirement for absolute radiometric calibration, the WFC must exhibit good radiometric stability to achieve its science objectives. It is expected that the WFC's radiometric response will vary by less than 1% per day. To monitor the radiometric stability and characterize long-term trends, a number of vicarious calibration activities are planned. These will be discussed in more detail in Section 6.0. A summary of the predicted WFC performance parameters are provided in Table 3.1

Table 3.1 WFC Performance Specifications.

Parameter	Specification	Comment
Bandpass	620-670 nm	Compatible with MODIS Channel 1
Single pixel IFOV	125 m x 125 m	24 μm pixels 135-mm focal length
Full Swath FOV	61 km	488 pixels cross-track
Dynamic Range	16 bits	Standard on CT-633
SNR at L_{max} (730 $Wm^{-2}\mu m^{-1}sr^{-1}$)	435	f/8 lens and full-well capacity of 150 ke^{-}
SNR at L_{typ} (12 $Wm^{-2}\mu m^{-1}sr^{-1}$)	51	As above

3.3 Instrument Operations

During the normal autonomous mode of operation, the WFC will acquire science data during the daylight portions of the CALIPSO orbits. Dark frame calibration data will be routinely acquired during the nighttime portions of the orbits. This nominal WFC duty cycle is shown in Figure 3.4. The data acquisition start and stop points on the orbit are defined by the solar elevation angle at the satellite. This value is programmable on-orbit. In addition to the autonomous mode, the WFC may also be operated in a raw data mode that will allow the full readout of all active pixels for diagnostic purposes. Further discussion of the dark frame calibration data and the diagnostic mode of operation are found in Section 6.1.

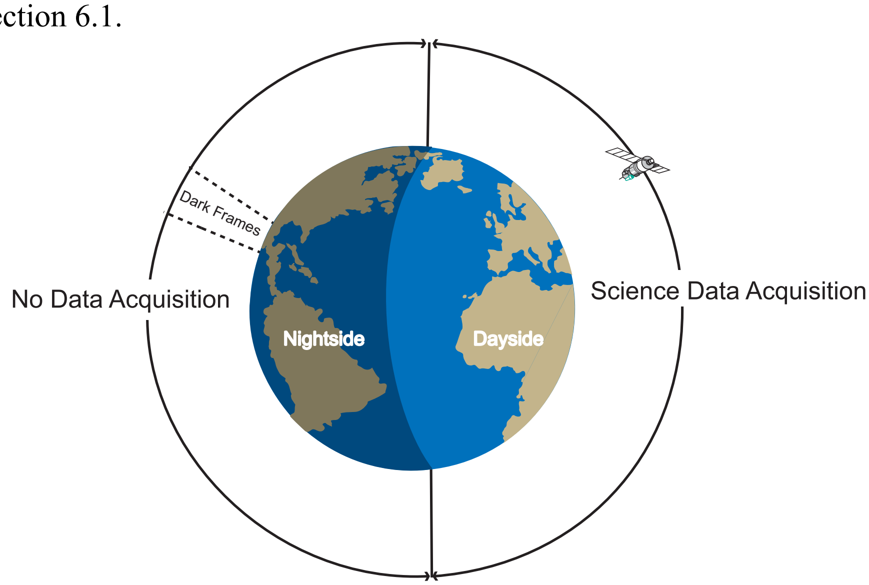

Figure 3.4. Standard duty cycle for WFC.

4. LEVEL 1 ALGORITHMS

The WFC Level 1 algorithms are designed to convert the raw Level 0 instrument data into radiometric parameters. To reduce the volume of data being down-linked from the CALIPSO satellite to the Earth, some averaging of the WFC Level 0 data is performed on orbit. However, the bulk of the processing is performed on the ground at the LaRC Atmospheric Sciences Data Center.

4.1 On-Board Processing

As discussed in Section 3.2, the WFC operates as a push broom line camera by reading out only one row of pixels per frame. During the CCD readout operations, pixels outside the central 5-km cross-track swath are binned on-chip to produce low-resolution (1 km x 125 m) image samples. The resultant single frame data consists of two low-resolution swaths (each 28-km wide) on either side of a high-resolution swath (5-km wide) centered on the orbit track covering 61 km across track and 125 m along track. There are a total of 96 image samples in each frame (56 low-resolution and 40 high-resolution). After each acquisition, these single frames are sent to the satellite Payload Controller for further processing and storage. The WFC single-frame processing is illustrated schematically in Figure 4.1.

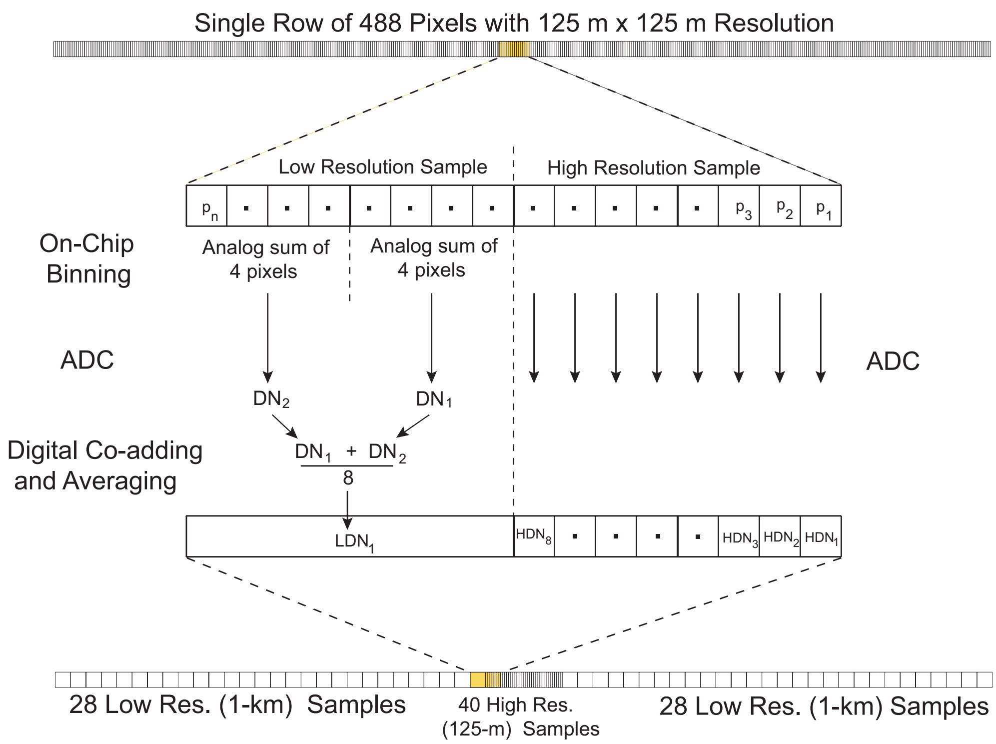

Figure 4.1. WFC single frame processing

At the Payload Controller, the WFC single frame data are collected and processed into WFC Major Profile packets that cover 5 km along track. As the single frames are collected, the two WFC low-resolution regions outside the central 5-km swath are additionally averaged in the along track direction to produce 1-km x 1-km low-resolution samples. No along-track averaging is performed on pixels in the central high-resolution swath and they retain their 125-m x 125 m resolution. This processing step is illustrated in Figure 4.2. The result of the Payload Flight Software (PFSW) on-board processing produces a 1-km along track by 61-km cross track image. The PFSW will buffer five of these processed 1-km x 61-km frames to produce the WFC Major Profile image that represents 5 km along track by 61 km across track. The Major Profiles are then formatted into data packets and stored in the Payload Mass Memory Module for transmission to the ground. The WFC is synchronized with the IIR such that eleven WFC Major Profiles correspond to each IIR image set (55 km along track). These Major Profiles will have a sequence count of 1 to 11. For the purposes of this document, the WFC Major Profile packets are considered to be the WFC Level 0 science data product that is input to the Level 1 processing.

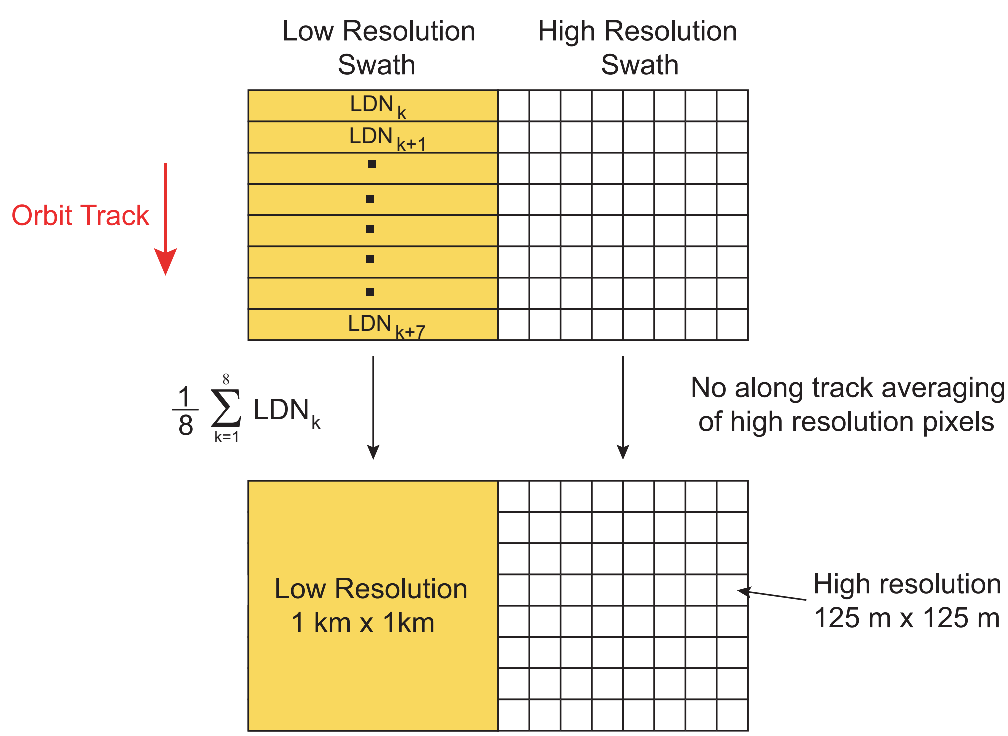

Figure 4.2. On-orbit processing of the WFC data by the Payload Flight Software.

4.2 Ground Processing

The WFC Level 0 data are transmitted from the satellite to the ground at least twice a day. Once received by the CALIPSO processing system at the Langley DAAC, the data are queued for Level 1 processing. The role of the Level 1 processing algorithm is to convert the WFC Level 0 science data into radiometric parameters and register the data onto a geometric grid. The Level 1 algorithms are described below.

4.2.1 Radiometric Conversion Algorithm

The radiometric conversion algorithm will convert the digital counts measured by the WFC into radiance values. For a given scene, the filtered radiance sensed by any active pixel p in the WFC CCD array can be expressed as

$$\tilde{I}_p = \int d\Omega F_p(\Omega) \int_{\Delta\lambda} d\lambda S(\lambda) I(\lambda)$$

where $F_p(\Omega)$ is the instrument field of view function that takes into account the instantaneous field of view for pixel p and spatial smearing; $S(\lambda)$ is the instrument response function that includes the detector quantum efficiency and any optical transmittance terms, including the filters and lens; $I(\lambda)$ is the unfiltered radiance from the scene at the top of the atmosphere before it enters the camera; and $\Delta\lambda$ is the band pass of the camera. The functional relationship between the filtered radiance and the digital counts measured by the WFC is given by

$$\tilde{I}_p = G\alpha_p [DN_p - DN_p^o]$$

where DN_p is the digital output of the WFC electronics in response to the incident radiance $\tilde{I}_p$, DN_p^o is the offset or background digital counts corresponding to the dark current in pixel p, α_p accounts for pixel to pixel variations in detector responsivity, and G is the system gain coefficient that relates absolute radiance to digital counts. Initial values for G, α_p, and DN_p^o will be determined through preflight laboratory tests of the WFC at Ball Aerospace & Technologies Corporation. On orbit, DN_p^o will be monitored through routine acquisition of dark frame data, while α_p and G will be monitored using vicarious calibration approaches. Details of the on-orbit calibration plan are found in Section 6.

4.2.2 Bi-Directional Reflectance

In addition to radiance, bi-directional reflectance will be derived from the WFC measurements. The bi-directional reflectance, ρ_p, from a given pixel is defined here as

$$\rho_p = \frac{\pi \tilde{I}_p}{\mu_o S_o}$$

where μ_o is the cosine of the solar zenith angle and S_o is the extraterrestrial solar irradiance over the WFC bandpass adjusted for the correct Earth-Sun distance. In terms of digital counts, the reflectance can be expressed as

$$\rho_p = \frac{G\alpha_p \pi [DN_p - DN_p^o]}{\mu_o S_o} \quad .$$

For the calculation of reflectance, the solar irradiance can be combined with G and α_p to form a general calibration constant, C_p, defined as

$$C_p = \frac{G\alpha_p}{S_o}$$

This approach will eliminate the dependence of the calibration on accurate knowledge of the solar irradiance over the WFC band pass. The calibration methodology is discussed further in Section 6.1.

4.2.3 Geolocation

The geolocation algorithms identify the Earth locations of the WFC measurements and define the solar and observational geometry of the measurements. These algorithms are implemented using the science data processing (SDP) toolkit provided by the Earth Observing System Data and Information System (EOSDIS) Core System (ECS) project. Using the SDP toolkit to calculate the WFC geometric parameters helps insure compatibility in Earth-spacecraft-Sun geometry when comparing WFC data with data from other instruments on the Aqua and other EOS spacecraft.

The required inputs for the geolocation processing are the CALIPSO navigation data that includes spacecraft attitude and ephemeris, UTC sample time, Earth rotation and ellipsoid models, and instrument pointing data. Spacecraft attitude is embedded in the Level 0 X-band telemetry; ephemeris is post-processed and transmitted from CNES; sample time is embedded in each CCSDS instrument packet. Pointing vectors for each WFC pixel will be determined during preflight testing. The latitude and longitude of each measurement is defined by the intersection of a given WFC pixel's pointing vector with the Earth ellipsoid. Earth location angles are reported in geodetic or geocentric coordinates. Viewing and solar zenith angles are also determined during the geolocation process. Error analysis for the geolocation algorithm is provided in the Theoretical Basis of the SDP Toolkit Geolocation Package for the ECS Project (ref. 3). Specified CALIPSO 3σ lidar geolocation errors are less than 1 km at nadir (Stadler, SER #JHS-007). Platform and payload pointing knowledge are allocated as a two dimensional horizontal error of 917 m (3σ) on the Earth's surface.

The following outline provides a high level summary of the geolocation process for each WFC pixel.

1. Generate the pixel pointing vector, **U,** in the spacecraft coordinate system (pointing vectors are derived from preflight test data)

2. Compute the required coordinate transformations

   a. Interpolate the spacecraft attitude to the time t the WFC image was acquired and construct the spacecraft-to-orbital coordinate transformation matrix $\mathbf{T}_{orb/sc}$

   b. Interpolate the ECI (Earth Centered Inertial) spacecraft position $\mathbf{P}_{eci}$ and velocity $\mathbf{V}_{eci}$ to image time t and construct the orbital-to-ECI transformation matrix $\mathbf{T}_{eci/orb}$

   c. Construct the ECI-to-ECR (Earth Centered Rotating) rotation matrix $\mathbf{T}_{ecr/eci}$ for the image time t

   d. Construct the composite transformation matrix $\mathbf{T}_{ecr/sc} = \mathbf{T}_{ecr/eci}\,\mathbf{T}_{eci/orb}\,\mathbf{T}_{orb/sc}$

3. Transform the instrument pointing vector and spacecraft position vector to ECR coordinates
   a. Transform the instrument pointing vector **U** to the ECR coordinate system $\mathbf{U}_{ecr} = \mathbf{T}_{ecr/sc}\,\mathbf{U}$
   b. Transform the spacecraft position vector $\mathbf{P}_{eci}$ to the ECR coordinate system $\mathbf{P}_{ecr} = \mathbf{T}_{ecr/eci}\,\mathbf{P}_{eci}$

4. Calculate intersection of the ECR pointing vector with the WGS84 ellipsoid

5. Convert the ECR ellipsoid lookpoint into geodetic or geocentric coordinates

6. Calculate viewing and solar zenith angles

The geolocation process will produce latitude and longitude coordinates for the 96 measurement samples in each WFC cross-track frame (40 high resolution and 56 low resolution). This product is referred to as the WFC "native" grid. Due to the sampling nature of the WFC, the along-track image will not have evenly spaced grid points.

4.2.4 Registration to IIR Grid

To facilitate the use of the WFC data in IIR retrievals, the WFC radiometric data will also be registered to the same Earth-based geometric grid as the IIR data. This grid projection has been defined by the IIR Mission Working Group as follows:

- Grid lines are orthogonal to the lidar track
- Center point in each grid line is aligned with the lidar track
- Center point is registered with a lidar shot
- Grid lines are separated by about 1 km, but exact sampling is determined by translation of sub-satellite point during a time Δt equivalent to 3 lidar shots (i.e. ~148 ms)

The WFC data are registered to the IIR grid by interpolation of the "native grid" data using a bilinear interpolation scheme.

4.2.5 Track and Swath Homogeneity

The WFC Level 1 data product will also include two parameters that quantify the homogeneity of the cross-track image frames: track homogeneity and swath homogeneity. The track homogeneity, T_h, is defined simply as the standard deviation in radiance over the central 5-km high-resolution portion of the WFC image frame normalized by the mean. Mathematically, it can be expressed as

$$T_h = \frac{\sigma(R_i)}{\overline{R}}$$

where R_i represents the 125-m resolution radiance measurements in the central 5-km portion of the WFC image and $\overline{R}$ is the corresponding mean radiance or reflectance in this same region. The track homogeneity will be calculated for each 125-m segment along the orbit track.

In a similar fashion, the swath homogeneity, S_h, is defined as the variance in radiance over the full 61-km cross-track swath normalized by the swath mean. The swath homogeneity will be calculated for each grid line in the IIR grid WFC data.

4.2.6 Input Data Requirements

The following is a list of all required input data for the WFC Level 1 processing.

WFC Level 0 Data (Major Profile Packets)

- Science data (digital counts)
- Housekeeping data (e.g., focal plane temperature, base plate temperature, etc.)
- CCD image location

Navigation Data

- Satellite ephemeris and attitude data
- Pointing vectors for target row of pixels
- UTC sample time
- Earth rotation and ellipsoid models

Sensor Artifact Data (determined prior to launch and updated as necessary)

- Dark current map
- Pixel defect map

Radiometric Calibration Data (determined prior to launch and updated as necessary)

- Calibration coefficients: C_p, G, α_p, S_o

4.3 Data Processing Flow

Figure 4.3 shows a top-level diagram of the WFC data processing flow from Level 0 digital numbers and engineering units through Level 1 data product generation. The steps can be summarized as follows:

1) Mask bad pixels using current pixel defect map
2) Subtract predetermined dark current offsets from Level 0 WFC data and apply calibration coefficients to produce radiances and reflectance
3) Geolocate WFC data using navigation data
4) Compute IIR grid and register WFC data to grid
5) Calculate track and swath homogeneity parameters
6) Write out Level 1 data product including current calibration coefficient file

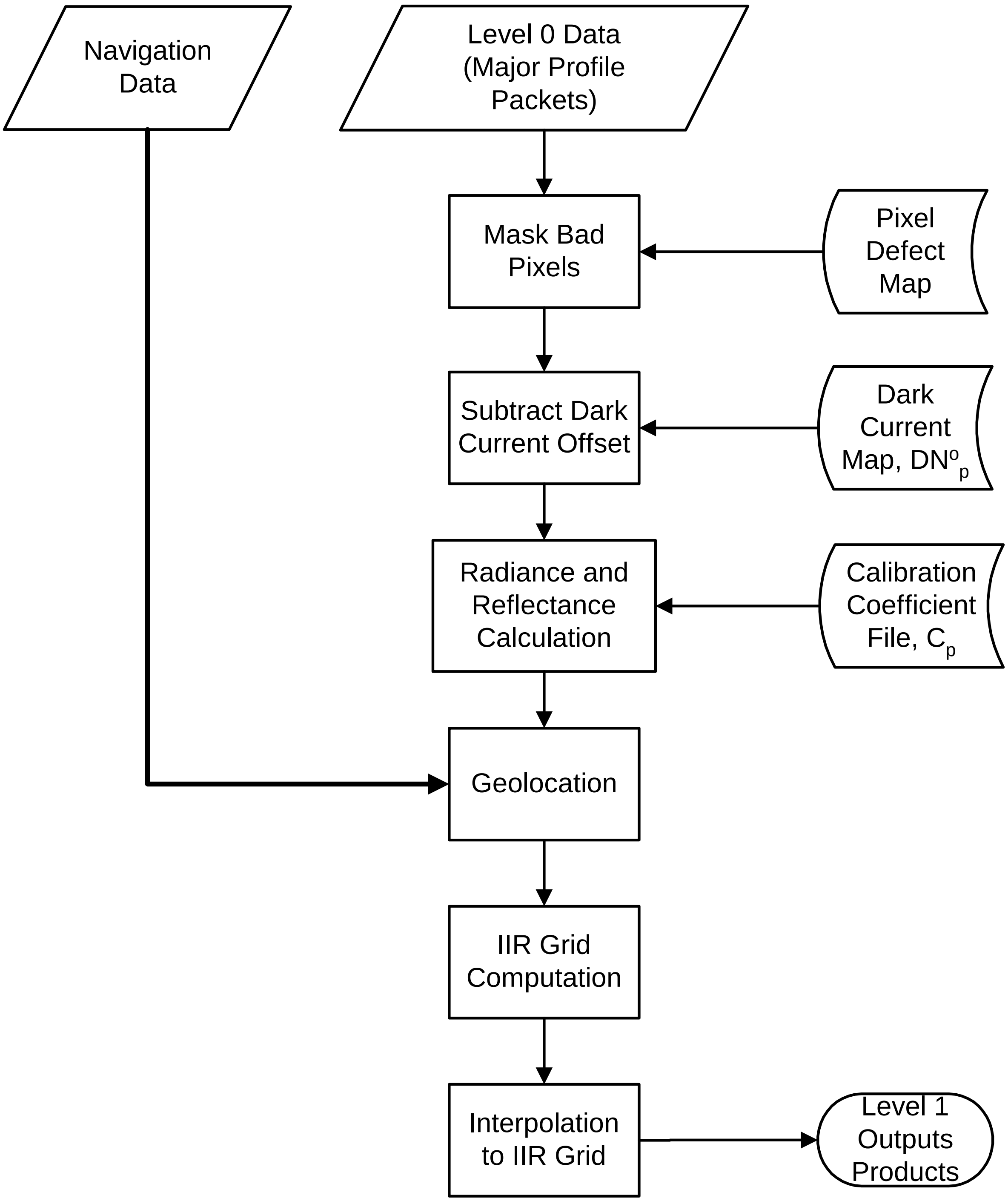

Figure 4.3. WFC Level 1 end-to-end data processing flow.

5. LEVEL 1 DATA PRODUCT

The WFC Level 1 data product will be archived at the LaRC Atmospheric Science Data Center. The CALIPSO Data Management Team will determine the format of the Level 1a data products.

5.1 Level 1 Product Content

The WFC Level 1 Data Product will consist of at least the following:

- **WFC 1-km x 1-km Gridded Earth View Data (IIR grid)**
  - Radiance
  - Reflectance
  - Swath Homogeneity
  - Position data (Latitude, longitude)
  - Viewing geometry

- **WFC 1-km x 1-km Gridded Earth View Data (native grid)**
  - Radiance
  - Reflectance
  - Swath Homogeneity
  - Position data (Latitude, longitude)

- **WFC 125- m x 125-m Gridded Earth View Data (central 5-km swath, native grid)**
  - Radiance
  - Reflectance
  - Track Homogeneity
  - Position data (Latitude, longitude)

- **Calibration Coefficients**
  - C_p
  - G
  - α_p

- **Housekeeping data**
  - Focal plane temperature
  - Base plate temperature

5.2 Browse Product

WFC browse images will be generated as part of the Level 1 data processing. The format of the browse images is TBD.

5.3 Calibration Product

Dark frame data will be collected on the night side of each orbit and will consist of the background (dark current) count levels in each pixel in the active row. Approximately 300 frames will be acquired each orbit. The orbital mean count levels and standard deviation will also be calculated for each pixel. This data will be reported as the *WFC Calibration Data Product* (see Section 6.2).

5.4 Raw Data Product

One of the WFC modes of operation is the "Raw Mode". In this mode, the WFC on-chip binning is turned off. The WFC controller will packetize the Raw Data directly from the WFC, with no binning performed by either the camera or the WFC controller software. Each packet of raw data will contain forty WFC images of 488 pixels each. This data will be reported as *WFC Raw Data Product*.

6. ON-ORBIT CALIBRATION MONITORING

The initial end-to-end calibration of the WFC will be determined during preflight ground testing of the instrument. The calibration of the instrument is expected to change during the mission and periodic on-orbit calibration will be required to monitor these changes and characterize long-term trends. The on-orbit calibration will be determined through a combination of multiple methodologies including vicarious calibration measurements, intercomparisons with Aqua instruments (primarily MODIS and CERES), and dark frame calibrations. The baseline approach for determining the time-dependent calibration coefficients is described below.

6.1 Radiometric Calibration

In the tropics, deep convective clouds with tops near the tropopause (~ 16 km) will be encountered frequently. These clouds represent the most stable, standard targets to monitor the end-to-end radiometric calibration of the WFC. Therefore, the baseline WFC calibration approach will be based on observations of tropical deep convective clouds.

6.1.1 Deep Convective Clouds as Vicarious Targets

Analysis of data from the Clouds and Earth's Radiant Energy System (CERES) experiment has shown that cold (i.e. optically thick with brightness temperatures < 205 K) tropical convective clouds possess uniform and stable reflectance properties that allow them to be used as shortwave calibration targets (references). For optical depths greater than a few hundred, cloud albedo becomes independent of the cloud optical depth. When viewed from above, these clouds are very bright and the albedo and angular scattering characteristics of these clouds are very uniform and stable from month to month (see Figure 6.1). Further, the reflectance is spectrally uniform. Additionally, due to their large vertical extent (cloud top heights > 12 km), aerosol and water vapor concentrations above these clouds are small and the atmospheric transmittance from satellite to cloud top can be estimated with high accuracy. Thus, these clouds represent excellent targets for vicarious radiometric calibration of the WFC. Results from the CERES analyses indicate that an adequate number of WFC cloud observations can be accumulated over a period of roughly six months that will allow monitoring of changes in the mean calibration over that period to within 4%.

In order to utilize cold convective clouds as vicarious calibration targets for the WFC, anisotropy will have to be carefully considered. Knowledge of the angular dependence of the WFC observations will be used to derive equivalent planetary cloud albedos that are independent of solar zenith angle. Then the observed cloud albedo can be compared with the predicted planetary albedo derived from similar satellite observations (i.e. AVHRR, GOES, VIRS, MODIS, ASTR) and theoretical model calculations. Unlike CERES which has a specific instrument designed for collecting anisotropy data, most narrowband instruments only perform cross-track scanning making it difficult to derive anisotropy models from these observations alone. As a result, a broadband-narrowband conversion scheme has been developed using CERES, VIRS, and MODIS observations on TRMM and Terra. Using this approach, it is possible to derive narrowband anisotropy models for the WFC from broadband models.

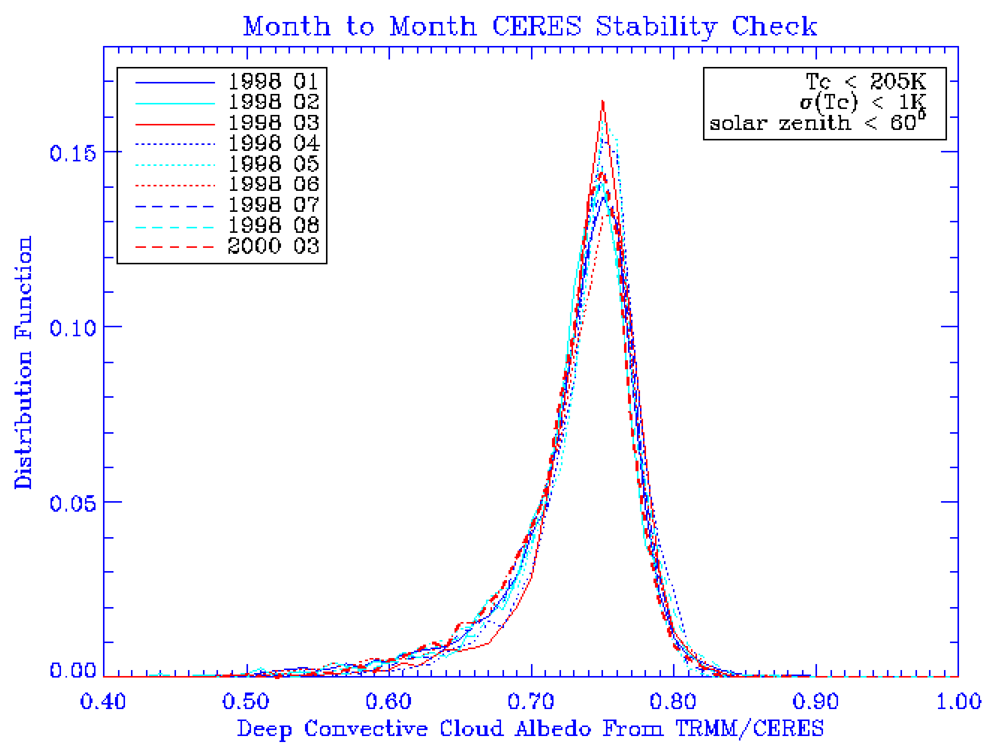

Figure 6.1. Distribution of monthly-averaged cloud albedo determined from CERES TRMM observations of deep convective clouds.

6.1.2 Radiometric Calibration Application

Consider the solar radiance reflected by a deep convective cloud. As observed by any WFC pixel, p, this radiance is expressed as

$$\tilde{I}_{cc,p} = G\alpha_p [\, DN_{cc,p} - DN_p^o \,] \quad .$$

Similarly, the bi-directional reflectance observed by any WFC pixel for this cloud is given by

$$\rho_{cc,p} = \frac{G\alpha_p \pi [\, DN_{cc,p} - DN_p^o \,]}{\mu_o S_o}$$

Rearranging terms and using the definition of the calibration constant, C_p, from Section 5.2.3, this expression can be written as

$$C_p = \frac{\mu_o \rho_{cc,p}}{\pi [\, DN_{cc,p} - DN_p^o \,]} \quad .$$

Therefore, if the cloud reflectance, $\rho_{cc,p}$, can be accurately characterized then cold tropical convective clouds could be used for determining the end-to-end radiometric calibration coefficient for the WFC. As shown by the CERES data, the cloud reflectance is very stable and we should be able to accurately characterize the angular variations using the well-calibrated shortwave MODIS channels. Although the extraterrestrial solar irradiance, S_o, is known to within 1 – 2 %, the absolute value is not required for determining the calibration constant. This also reduces the calibration errors due to uncertainty in knowledge of the WFC spectral band pass.

Operationally, the time-dependent calibration coefficient, C_p, will be determined by combining and averaging tropical cloud measurements made over multiple orbits. To achieve the desired accuracy, averages of several months of measurements may be required.

6.1.3 Other Vicarious Approaches

Vicarious calibration requires stable, homogeneous targets with relatively high reflectance. Additional potential calibration targets for the WFC include deserts, polar snow, and oceans.

Deserts

Well-characterized land surfaces may also be used as calibration targets under clear sky conditions. Deserts make good targets because they tend to be homogeneous over large regions and stable with time, but their angular scattering properties must be well characterized. Potential desert targets include portions of the Sahara desert in Algeria that have been characterized for use in calibrating the POLDER instrument and areas in the Australian desert which are uniform and have been, or could be, characterized. Desert targets also pose several potential problems for accurate calibration. For instance, it is not clear how accurately the scattering properties of the desert surfaces can be characterized, but probably nowhere close to the 2% level. Additionally, the presence of aerosol and water vapor can make accurate atmospheric transmissivity calculations problematic. POLDER claims a calibration to 4% accuracy using vicarious techniques, but in this case desert scenes are only used for calibrating the angular variation of the responsivity, not absolute radiometric calibration.

Polar Snow

Snow covered surfaces in the polar regions also could be used as vicarious calibration targets. Snow covered surfaces tend to be very homogeneous and offer the advantage that a large number of samples could be collected during most orbits. One difficulty in using snow surfaces as calibration targets is the solar zenith dependence varies with the age of the snow. In addition, the presence of Arctic haze and low level clouds can frequently contaminate the calibrations. A solar zenith dependence database for snow surfaces has been produced from MODIS Terra data.

Oceans

Ocean surfaces also might be useful calibration targets. In this case, the CALIPSO lidar can be used to identify clear ocean scenes with low aerosol loading. In contrast to cold convective clouds, deserts, and snow, these will be low-radiance scenes. At low wind speeds and outside of Sun glint regions, the oceans surface is extremely dark at 650 nm and the WFC signal will be dominated by Rayleigh scattering which is well-known. The small contribution from scattering off the ocean surface can be estimated with reasonable accuracy and the contributions from aerosols can be estimated from the lidar observations.

6.1.4 Cross-Calibration with MODIS and CERES

Since MODIS has a well-calibrated shortwave channel centered very near 645 nm, it may be possible to use tropical convective clouds to transfer the MODIS calibration to the WFC. One potential difficulty is the differences in viewing geometry between CALIPSO and Aqua. As shown in Figure 6.2, the reflectance for viewing zenith angles between 0 – 5 degrees very similar to those for viewing angles between 5 – 10 degrees. Therefore, if the CALIPSO and Aqua orbits are close, the reflectance should be almost identical. However, if the orbits differ significantly, then viewing zenith dependence will need to be considered. The narrowband angular reflectance characteristics of cold tropical clouds may be derived from MODIS measurements.

Comparison of the WFC observations with the CERES broadband reflectance may also prove useful. For example, Figure 6.3 shows the relationship between CERES broadband and VIRS narrowband (650 nm) reflectance based on TRMM observations of ice clouds. The solar zenith angle in this case is between 42 – 48 degrees. The straight line in the figure is derived from model calculations with assumed particle shapes. Similar comparisons of the WFC data and the CERES Aqua broadband shortwave observations may provide useful calibration information. Again, however, viewing angle differences between the CALIPSO WFC and Aqua CERES may have to be considered.

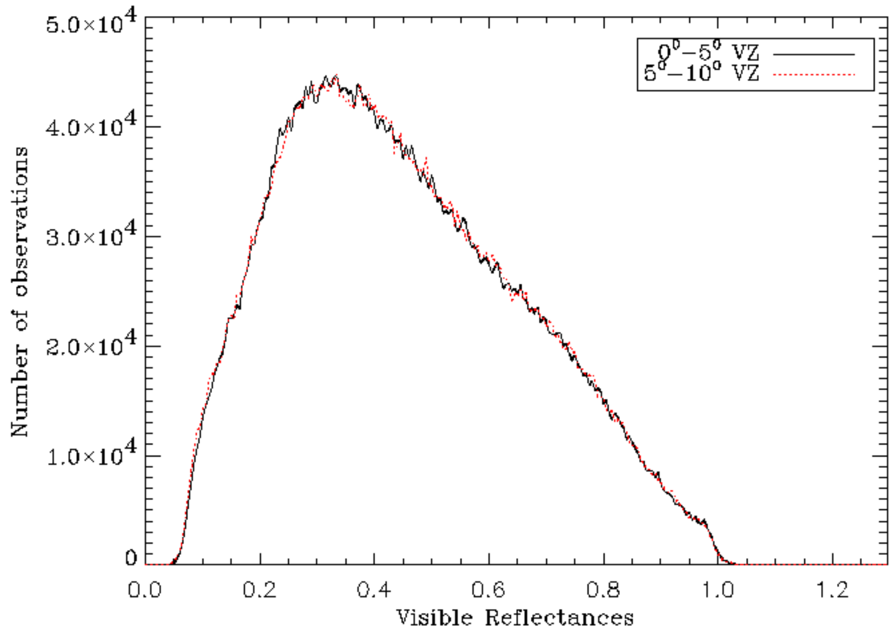

Figure 6.2. Comparison of visible reflectance for viewing angles between 0–5^o and 5-10^o.

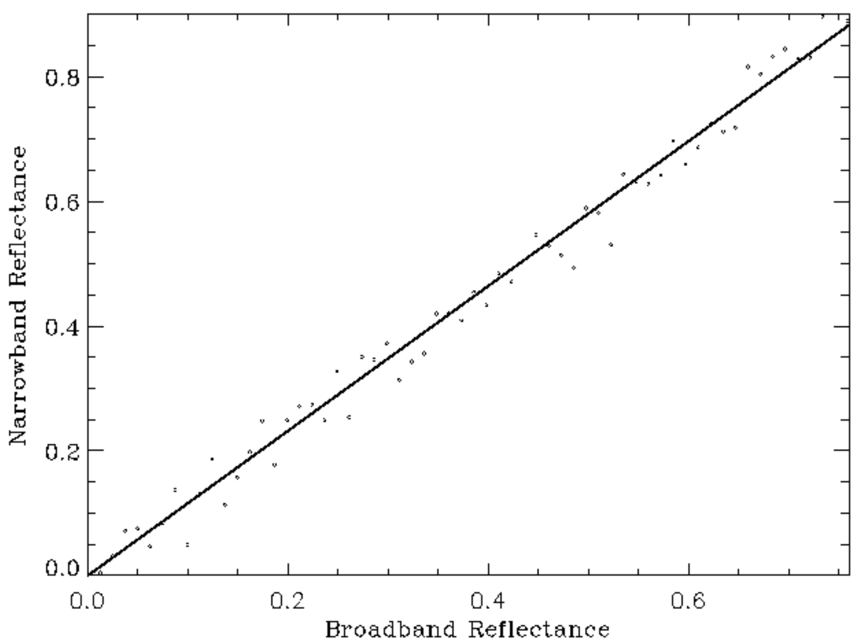

Figure 6.3. Comparison between CERES broadband and VIRS narrowband cloud reflectance (solid line represents model calculations with assumed particle shapes).

6.2 Dark Current Offset

The dark current offset, DN_p^o, is essentially the thermally induced charge accumulated by each detector pixel when no light is present. Preflight values of these offsets will be determined during ground testing of the WFC. However, radiation effects in space are expected to severely degrade the dark current over the lifetime of the mission. In addition, although the CCD focal plane temperature is controlled by a thermoelectric cooler (TEC), temperature fluctuations may occur due to strong thermal gradients across the spacecraft platform. Therefore, it is important that the dark current offset be monitored carefully on orbit.

Nominally, dark frames will be acquired during the nighttime portion of each orbit to calibrate the dark current offset in each pixel. Approximately 300 dark frames will be acquired during each orbit. The Level 0 dark frame data will have the same format as the daylight science data, but will have a flag in the header record to distinguish it from daytime science data. Operationally, the dark frame data will be processed as part of the Level 1 data processing and reported as the *WFC Level 1 Calibration Data Product*. The calibration data will consist of the background count levels in each pixel for each frame. In addition, the mean count levels and standard deviations will be calculated for each orbit. The calibration data will be analyzed off-line to monitor changes in the dark current offset and identify defective pixels. Trends in the data will be noted and the dark current file used in Level 1 processing will be updated as necessary.

7. LEVEL 1 QUALITY CONTROL

7.1 Geolocation Verification

Verification of the WFC pixel geolocation accuracy and an assessment of the spacecraft pointing will be performed using a coastline-crossing algorithm. This pointing assessment algorithm was first used on ERBE (Hoffman et al. 1987) and further refined in support of the CERES instrument Tropical Rainfall Measuring Mission (TRMM) (Currey et al. 1998). Validation of the geolocation process requires comparison of detected Earth features with a database containing the same features independently geolocated. For CALIPSO, clear coastline scenes will be analyzed to determine coastline-crossing locations. These are then compared with a coastline map to assess overall pointing accuracy. A large number of independently processed coastline scenes will be analyzed to detect systematic biases in the spacecraft along-track and cross-track coordinate system.

7.1.1 Coastline Crossing Algorithm

As a detector scans across a high contrast scene, such as desert adjacent to ocean, a step response similar to Figure 7.1 is produced. The coastline signature is modeled using a cubic fit of four contiguous measurement samples

$$y_i = ax_i^3 + bx_i^2 + cx_i + d$$

where y_i is the measured radiance and x_i is pixel position (latitude or longitude). The equation coefficients are determined by solving the system of equations

$$\begin{bmatrix} a \\ b \\ c \\ d \end{bmatrix} = \begin{bmatrix} x_1^3 & x_1^2 & x_1 & 1 \\ x_2^3 & x_2^2 & x_2 & 1 \\ x_3^3 & x_3^2 & x_3 & 1 \\ x_4^3 & x_4^2 & x_4 & 1 \end{bmatrix}^{-1} \begin{bmatrix} y_1 \\ y_2 \\ y_3 \\ y_4 \end{bmatrix}$$

The inflection point, $-b/3a$, is considered to be the location of the coastline if it falls between x_2 and x_3 and the change in the observed radiance (or reflectance) exceeds a predefined threshold.

The geolocation error for a scene is calculated by fitting an ensemble of detected crossings to a corresponding coastline map. The shift in geographical coordinates required to minimize the distance between the calculated coastline crossings and the coastline map is defined as the geolocation error for an individual scene. Figure 7.2 depicts an ensemble of crossings simulated from a digitized map of Baja, California with a bias of -1.2^{o} longitude and 0.2^{o} latitude. The downhill simplex minimization algorithm (reference 5) iteratively shifts the coastline in three separate directions until the differences between the calculated crossings and the map coastline are minimized. Geographic errors are transformed into spacecraft cross-track and along-track coordinates. Additional scenes are required to identify and track systematic biases in the instrument/satellite system.

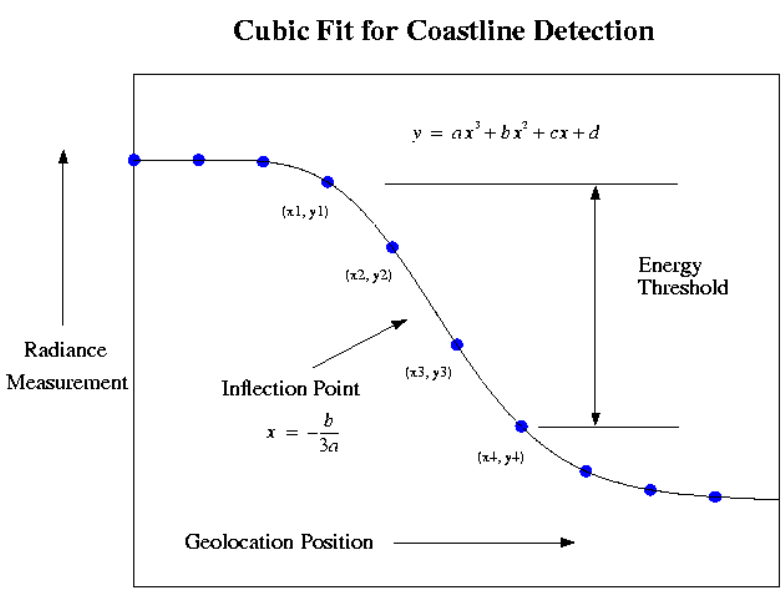

Figure 7.1. Determination of coastline crossing location.

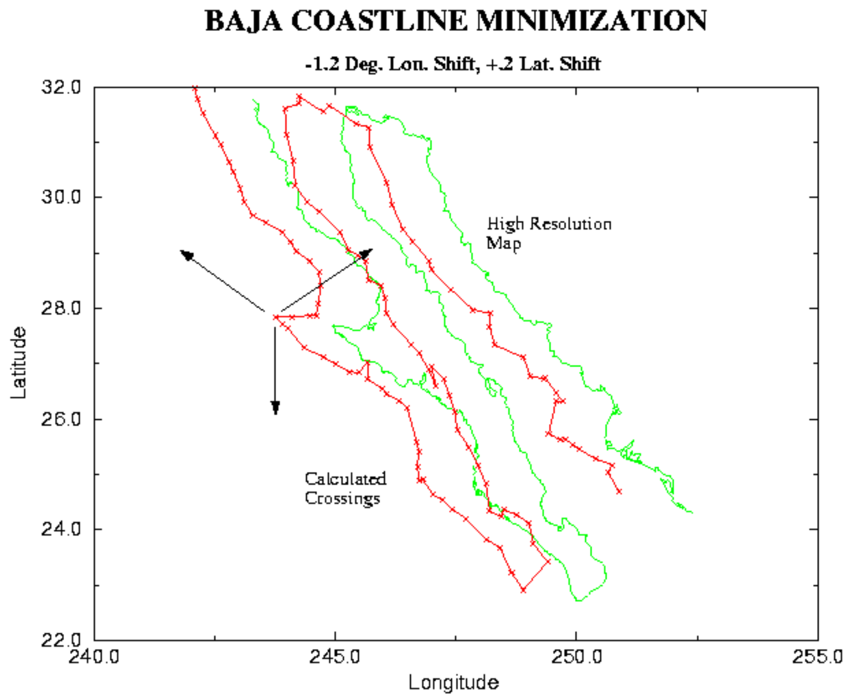

Figure 7.2. Minimization technique to determine geolocation error.

Figure 7.3 shows an example of this technique applied to a TRMM Visible and Infrared Scanner (VIRS) image of the western coast of Mexico taken January 3, 1998. Spacecraft heading is –31.6° relative to the equator. The minimum brightness temperature threshold in this case is 3 K. The coastline fitting technique minimizes 218 detected crossings to the World Data Bank II map database. The resulting longitude error of –0.0011° and latitude error of –0.0041° correspond to an along track error of 133 m and a cross track error of 455 m. VIRS pixel resolution is 2 km.

7.1.2 Algorithm Uncertainty Considerations

7.1.2.1 Coastline Detection Errors

The detector point spread function (PSF), coastline response model, and random sampling all affect the uncertainty of the calculated crossing location. Figure 7.4 depicts a number of theoretical one-dimensional PSFs with their corresponding step responses. Increments in the x-axis or along-scan direction are 0.01 pixels. The normalized PSFs vary from one to four pixels in width. The coastline truth is simulated with a step input at pixel index 100.

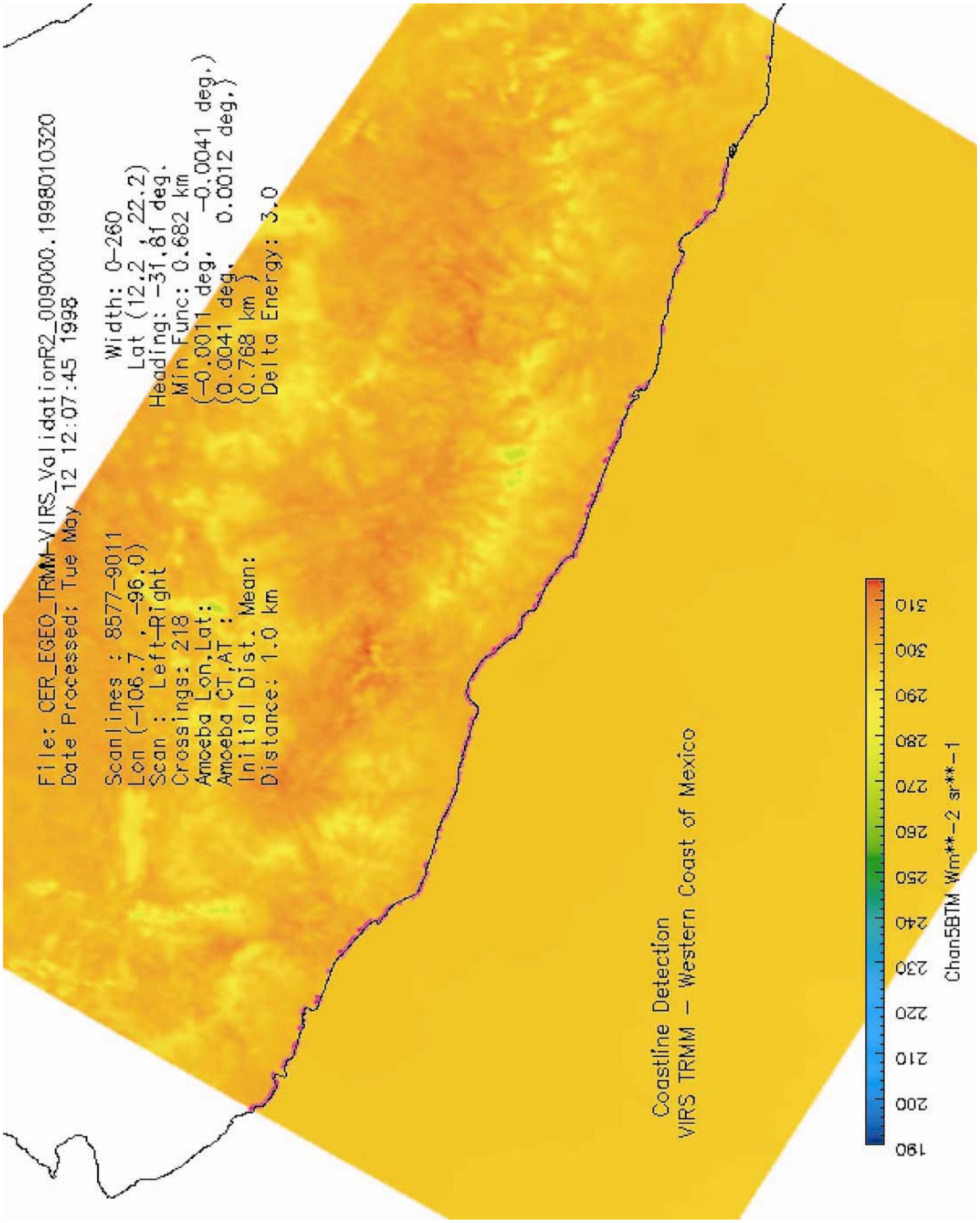

Figure 7.3. VIRS coastline detection example, Mexico, January 3, 1998

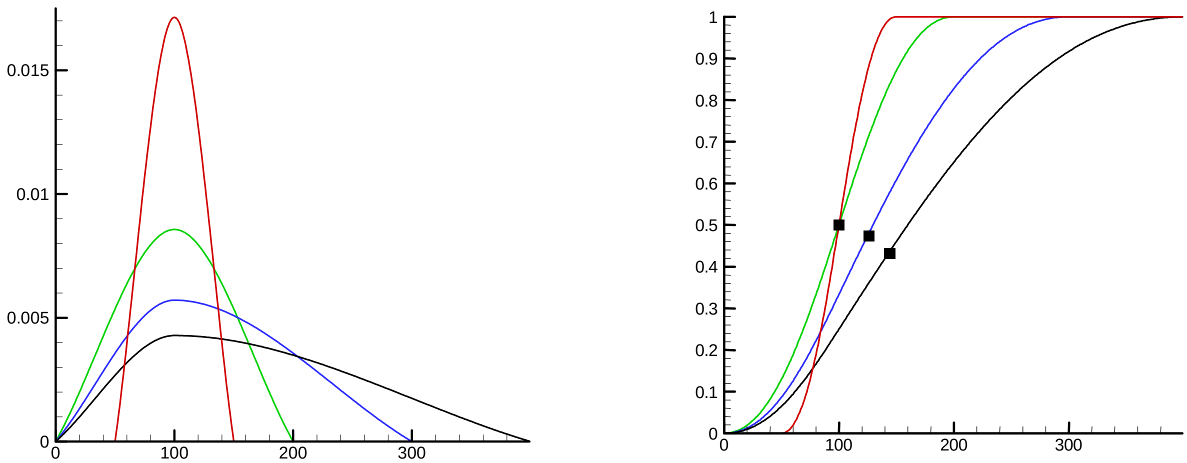

Figure 7.4. One dimensional PSFs and step response inflection point shifts.

Inflection points are calculated from four equally spaced random samples. Calculated crossings are compared to the true simulated coastline at pixel index 100. Non-symmetric PSFs have shifts of 0.27 and 0.45 pixels with σ = 0.06 pixels. Table 7.1 summarizes the PSF coastline detection biases and uncertainties (N=100 random samples). Given a step input to simulate an ideal coastline and a detector with a symmetric PSF, the location of the detected crossing should be within 0.5 pixels (3σ) of the true crossing.

PSF Width (pixels)	Shift (pixels)	σ (pixels)	3σ (pixels)
1	0.000	0.176	0.528
2	0.000	0.098	0.294
3	0.266	0.055	0.165
4	0.446	0.064	0.192

Table 7.1. PSF step response coastline detection biases and uncertainties

As a test case, a visible radiance land/water scene was generated using a radiative transfer model. This 1-m resolution dataset serves as the coastline truth. A convolution with the two-dimensional WFC PSF produces a simulated 125-m resolution, 5-km wide WFC scene. Figure 7.5 shows the 37 crossings detected from the 125-m data compared to the true coastline. Table 7.2 presents the along-track errors for the processed simulated WFC scene. The mean shift is 0.024 pixels (3 m) with 99.7% of the detected crossings within

0.28 pixels (35 m) of the true coastline. A mean negative shift indicates that the calculated crossings occur prior to the coastline map locations. To detect both along-track and cross-track errors, the minimization technique described in section 7.1.1 will be used.

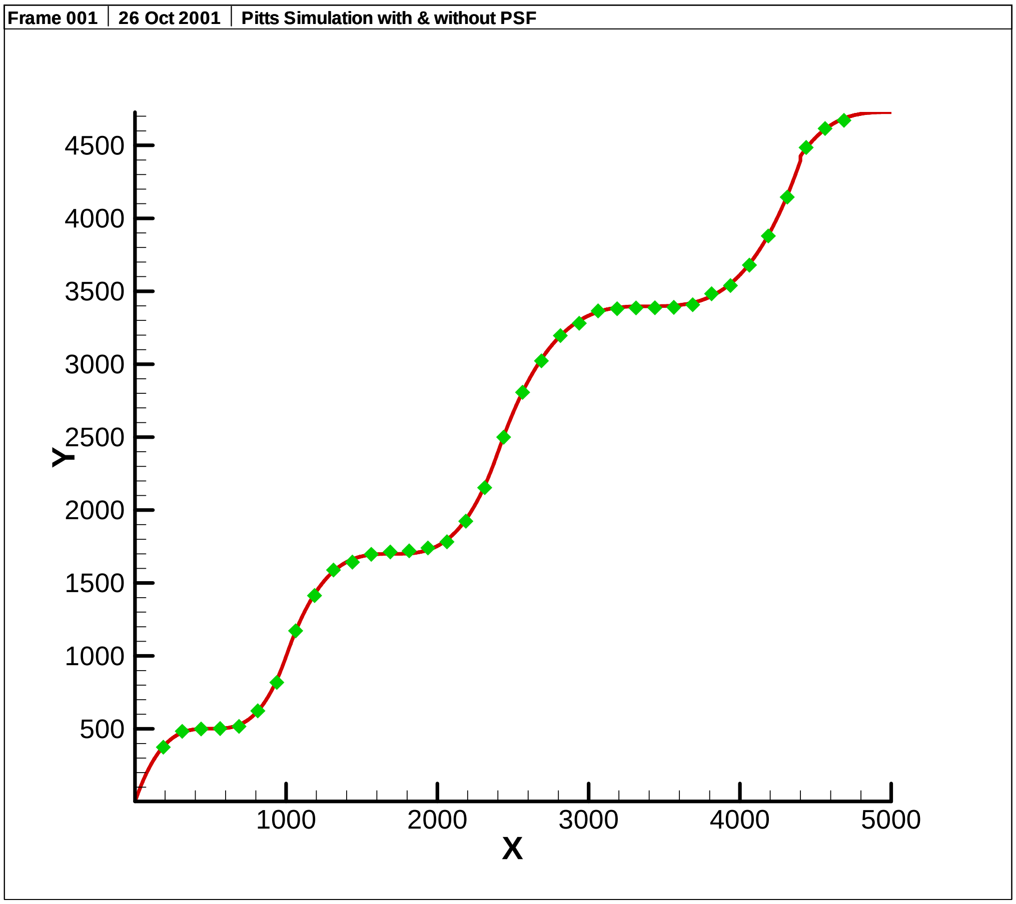

Figure 7.5. WFC scene simulated w/ 2D PSF convolution

Shift (pixels)	σ (pixels)	3σ (pixels)
-0.024	.084	.253

Table 7.2. Along-track errors for simulated WFC scene

7.1.2.2 Bias Determination Error

The bias determination algorithm calculates the longitude and latitude error for each ensemble of crossings. The coastline detection algorithm essentially samples the shape of a coastline; the minimization process matches this shape to a reference map. This section attempts to quantify the uncertainty of the bias determination algorithm and define map resolution and accuracy requirements.

Table 7.3 depicts the bias determination accuracy when geographic biases are added to crossings simulated from a reference map, in this case a map of Baja, California containing 1158 values. Biases between the crossings and the map range from 1.2 degrees (~133 km) to .0001 degrees (~11 m). In all cases, except for the ridiculous case of only 4 crossings, the correct bias is determined. The final average simplex shift indicates the magnitude and direction the crossings must be shifted in geographic coordinates to minimize the average crossing distance to the map. The simplex shift is the negative bias for a scene. The crossings are shifted back to their original map positions to within one meter (final difference). A fractional convergence tolerance, ftol, of .01 requires the three simplex values to agree to within 1% of each other. Reference 5 provides an excellent description of the downhill simplex method of minimization.

The minimization process also works when the map resolution is less than the instrument pixel resolution. The ratio of map points per scene to crossings detected varies from 1 to 40 with accurate bias detection. Further investigation is required before selecting a map for CALIPSO WFC geolocation assessment. The World Data Bank II database provides a maximum of 3 km spacing between successive points. No accuracy numbers are provided with the data generated by the CIA in 1995. The uncertainty of the bias determination algorithm is assumed to be the same as the map accuracy.

7.1.2.3 Geolocation Assessment Error

The geolocation assessment accuracy is determined from the uncertainties of the coastline detection and bias determination algorithms. The coastline detection uncertainty, σ_{cd}, is .084 pixels for the WFC scene simulated using a two dimensional PSF. The bias determination uncertainty, σ_{bd}, is determined from the map accuracy which is estimated at 100 m. For 125 m pixels the geolocation assessment uncertainty, σ_{ga}, is estimated as $\sigma_{ga}^2 = \sigma_{cd}^2 + \sigma_{bd}^2$; σ_{ga} is 0.80 pixels (100.6 m). Assuming a map uncertainty of 50 m, σ_{ga} decreases to 0.41 pixels (51.1 m).

7.1.2.4 ASTER Processing

The coastline geolocation assessment algorithm will be tested using Band 2 (0.63 – 0.69 μm) 15-m Visible Near Infrared (VNIR) L1A ASTER data. Test results will confirm theoretical uncertainties estimated in section 7.1.2.3 and aid in selecting an appropriate map.

7.1.2.5 Post Launch Bias Monitoring

During the first month post launch the actual uncertainty of the process, σ'_{GA}, will be determined empirically. Assuming a high accuracy map is located, the uncertainty of the geolocation assessment process should be less than 0.5 pixels. Each month following, geolocation biases will be monitored and, if needed, be corrected in the production processing system.

7.2 Detection of Defective Pixels

Pixels typically will fail in one of two ways: as a dead pixel that exhibits no charge or as a bright pixel that exhibits large charge independent of the incident illumination. Both of these pixel defects will be obvious in the image data. A dead pixel will appear as dark streak in the data while a bright pixel will appear as a bright stripe in the data. In addition, both types of pixel defects will be identified through statistical analysis of the dark frame data.

Dead pixels will not affect adjacent pixels. Bright pixels will have essentially no effect on pixels in adjacent columns because the CCD has channel-stop regions to isolate columns from one another. However, charge from bright pixels may bleed into adjacent rows. If isolated pixels fail, they will be added to the bad pixel map and masked during Level 1 processing. If multiple pixel failures occur in the active row, then the target row will be moved. In the case of bright pixels, the target row will be shifted by at least 2 rows to reduce the bleeding effect.

8. REFERENCES

1. Release 5A SDP Toolkit Users Guide, ECS 333-CD-500-001, June 1999
2. L. Hoffman, W. Weaver, J. Kibler, “Calculation and Accuracy of ERBE Scanner Measurement Locations,” *NASA Technical Paper 2670*, 1987
3. P. Noerdlinger, Theoretical Basis fo the SDP Toolkit Geolocation Package for the ECS Project, ECS 445-TP-0002-002, May 1995
4. C. Currey, L. Smith, B. Neely, “Evaluation of Clouds and the Earth’s Radiant Energy System (CERES) scanner pointing accuracy using a coastline detection system,” SPIE Conference on Earth Observing Systems III, San Diego, CA, July 1998

Table 7.3. Scene Bias Determination Uncertainty

Number Xings	Lon, Lat Data Bias (lon,lat)	Start Simplex (degrees)	Final Average Simplex Shift (lon,lat)	Y[0] (m)	ftol	Number Function Calls	Number Simplex Movements	Converge
1158 (÷1)	(0, 0)	+/- 1.0	(-5.542168e-09, -6.309288e-08)	0.017	.001	217	97	yes
116 (÷10)	(0, 0)	+/- 1.0	(-2.601026e-08, -5.096325e-08)	0.018	.01	1000	886	no
39 (÷30)	(0, 0)	+/- 1.0	(-8.514351e-08, 1.417804e-07)	0.010	.01	128	64	yes
1158 (÷1)	(1.2, 0.2)	+/- 2.0	(-1.199997e+00, -2.000005e-01)	0.364	.01	108	57	yes
116 (÷10)	(1.2, 0.2)	+/- 2.0	(-1.199997e+00, -2.000002e-01)	0.405	.01	112	59	yes
29 (÷40)	(1.2, 0.2)	+/- 2.0	(-1.199997e+00, -2.000004e-01)	0.268	.01	123	65	yes
1158 (÷1)	(-0.2, 1.2)	+/- 2.0	(1.999972e-01, -1.200000e+00)	0.366	.01	113	59	yes
6 (÷200)	(-0.2, 1.2)	+/- 2.0	(1.999969e-01, -1.200001e+00)	0.355	.01	134	67	yes
4 (÷300)	(-0.2, 1.2)	+/- 2.0	(1.077308e+00, -2.743792e+00)	10710.0	.01	45	21	yes
58 (÷20)	(-0.5, -0.5)	+/- 1.0	(5.000001e-01, 5.000002e-01)	0.016	.01	112	58	yes
58 (÷20)	(0.5, -0.5)	+/- 1.0	(-4.999998e-01, 5.000002e-01)	0.018	.01	112	56	yes
58 (÷20)	(-0.01, -0.01)	+/- 1.0	(9.994982e-03, 1.000023e-02)	0.433	.01	101	54	yes
58 (÷20)	(-0.01, -0.01)	+/- 1.0	(-9.995032e-03, 9.999918e-03)	0.659	.01	108	57	yes
1158 (÷1)	(0.001, -0.001)	+/- 2.0	(-1.002690e-03, 1.000781e-03)	0.743	.01	93	50	yes
39 (÷30)	(0.001, -0.001)	+/- 2.0	(-1.005811e-03, 9.998169e-04)	0.657	.01	107	58	yes
1158 (÷1)	(0.0001, 0.0001)	+/- 0.5	(-1.049436e-04, -9.997992e-05)	0.717	.01	93	48	yes
58 (÷20)	(0.0001, 0.0001)	+/- 0.5	(-1.066786e-04, -9.977541e-05)	0.561	.01	99	51	yes